Ion Distributions near a Liquid-Liquid Interface

Guangming Luo,[1] Sarka Malkova,[1] Jaesung Yoon,[1] David G. Schultz,[1,2] Binhua Lin,[3] Mati Meron,[3] Ilan Benjamin,[4] Petr Vanýsek,[5] Mark L. Schlossman[1,2]*

Mean field theories of ion distributions, such as the Gouy-Chapman theory that describes the distribution near a charged planar surface, ignore the molecular-scale structure in the liquid solution. The predictions of the Gouy-Chapman theory vary substantially from our x-ray reflectivity measurements of the interface between two electrolyte solutions. Molecular dynamics simulations, which include the liquid structure, were used to calculate the potential of mean force on a single ion. We used this potential of mean force in a generalized Poisson-Boltzmann equation to predict the full ion distributions. These distributions agree with our measurements without any adjustable parameters.

Ion distributions in electrolyte solutions near charged interfaces underlie processes as diverse as electron and ion transfer at biomembranes and redox processes at mineral-solution interfaces and also influence many practical applications in analytical chemistry and electrochemistry. Ion distributions near a charged, planar surface can be predicted by Gouy-Chapman theory, which solves the Poisson-Boltzmann equation with simplifying assumptions (*1*, *2*). This theory considers point-like ions interacting via their mean field in a solvent that is treated as a structureless continuum, ignoring its molecular-scale structure.

Extensive development of theory has addressed the limitations of the Gouy-Chapman theory (*3*) and predicted that deviations are largely a result of the difference between the interfacial and the bulk liquid structure. However, few experimental probes are directly sensitive to the structure near the charged interface, and the limits of the validity of the Gouy-Chapman theory have not been properly tested. Our structural measurements, which demonstrate the failure of Gouy-Chapman theory, are in agreement with predictions based upon a molecular dynamics simulation that includes the effects of interfacial liquid structure.

The Poisson-Boltzmann equation is used to describe ion distributions near electrified interfaces:

$$\frac{d}{dz}\varepsilon(z)\frac{d}{dz}\phi(z) = -\sum_i e_i c_i^{o} \exp[-\Delta E_i(z)/k_B T] \quad (1)$$

where $\phi(z)$ is the electric potential at a distance z from the interface, $\varepsilon(z)$ is the permittivity function, e_i and c_i^{o} are the charge and bulk concentration of ion i, respectively, $\Delta E_i(z)$ is the energy of ion i relative to the bulk phase, and $k_B T$ is Boltzmann's constant times the temperature. The Gouy-Chapman or Debye-Hückel theories of ion distributions assume that E_i depends only upon the electrostatic energy, such that $E_i(z) = e_i\phi_i(z)$, and that the permittivity function is given by a constant bulk value, $\varepsilon(z) \equiv \varepsilon$. However, structural properties of the liquid, such as the ion or solvent sizes and interactions between ions and solvent molecules, that are ignored can lead to packing effects and correlations (ion-solvent, solvent-solvent, and ion-ion) that influence the ion free energy. The liquid structure can be included formally by expressing $E_i(z)$ as $E_i(z) = e_i\phi_i(z) + f_i(z)$, where $f_i(z)$ is a free energy profile of ion i that describes the correlations (*4*, *5*). We show that the potential of mean force calculated by molecular dynamics (MD) simulations for a single ion in a solvent near an interface can be a good approximation for $f_i(z)$.

Classical electrochemical measurements have discovered inadequacies in the Gouy-Chapman theory. Capacitance measurements as a function of applied bias potential at the liquid-liquid interface depend upon the ionic species (*6*), in contradiction with the Gouy-Chapman theory, for which only the ionic charge is relevant. In addition, the shape and the magnitude of the capacitance as a function of interfacial potential are often in disagreement with Gouy-Chapman theory (*7*, *8*). A Stern layer of preferentially adsorbed solvent molecules or ions is often used to explain measurements at the solid electrode–electrolyte solution interface (*9*). The Gouy-Chapman-Stern theory includes the adsorbed layer plus the diffuse ion distribution described by the Gouy-Chapman theory. Preferential adsorption of ions can occur at the liquid-liquid interface, although tension measurements demonstrate that this does not occur for the samples studied here (*10*).

Few experimental techniques can probe ion distributions in solutions near interfaces. The surface scattering of x-rays and neutrons is, in principle, sensitive to this distribution. In particular, several x-ray studies have explored the electrical double layer for different geometries. Bedzyk *et al.* used long-period x-ray standing waves to study the double layer adjacent to a charged phospholipid monolayer adsorbed onto a solid surface (*11*). Their data were consistent with an adsorbed Stern layer and a diffuse layer described by the linearized Gouy-Chapman theory, which predicts an exponentially decaying charge distribution.

A number of x-ray studies have probed the structure of the Stern layer due to counterion adsorption to a Langmuir monolayer on the surface of water but did not make conclusions about the diffuse (or Gouy-Chapman) part of the ionic distribution (*12*–*14*). One of these studies (*14*) suggested the presence of additional ions further from the surface than the Stern layer. Fenter *et al.* used Bragg x-ray standing waves and surface x-ray absorption spectroscopy to probe the structure within the adsorbed (Stern) layer of an electrolyte solution on a mineral surface. They determined (*15*) roughly the partitioning of the ions between the adsorbed layer and the diffuse charge layer but could not probe the form of the ion distribution. Recent small-angle x-ray scattering studies of counterion condensation around DNA found agreement with solutions of the nonlinear Poisson-Boltzmann equation for this geometry that included an atomic model of the DNA (*16*). Further studies by this same group (*17*) provided indirect evidence that ion size needs to be considered in the Poisson-Boltzmann treatment.

The liquid-liquid interface has several advantages over other interfaces for the investigation of ion distributions. It does not impose an external structure on the adjacent liquid as might be expected from the atomic-scale corrugations on a solid surface. A solid surface or a Langmuir monolayer on the water surface often has bound charges whose charge density is unknown but must be determined by the experiment in addition to determining the diffuse ion distribution. Also, the use of large organic ions in the organic phase at a liquid-liquid interface is advantageous for structural determination.

We formed liquid-liquid interfaces between an aqueous solution of hydrophilic ions and a polar organic solution of hydrophobic ions. The ions form back-to-back electrical double layers. Solutions were prepared at a concentration of 0.01 M tetrabutylammonium tetraphenylborate (TBATPB) in nitrobenzene and concentrations of 0.01, 0.04, 0.05, 0.057, and 0.08 M tetrabutylammonium bromide (TBABr) in purified water (*18*). Upon equilibration, the ions partition between the two phases until the electrochemical potential for each ion is equal in both phases. Use of a common ion, in this case TBA^+, whose concentration in both bulk phases is comparable, allows the electric potential across the liquid-liquid interface to be varied by adjusting the concentration of TBABr at a fixed concentration of TBATPB (*19*). We calculated the ion partitioning and the interfacial electric potential with the use of the Nernst equation and the standard Gibbs free energy of transfer of an ion from water to nitrobenzene (table S1) (*18*).

[1]Department of Physics, [2]Department of Chemistry, University of Illinois at Chicago, Chicago, IL 60607, USA. [3]Center for Advanced Radiation Sources, University of Chicago, Chicago, IL 60637, USA. [4]Department of Chemistry, University of California, Santa Cruz, CA 95064, USA. [5]Department of Chemistry and Biochemistry, Northern Illinois University, DeKalb, IL 60115, USA.

*To whom correspondence should be addressed. E-mail: schloss@uic.edu

X-ray reflectivity from the liquid-liquid interface was measured at the Chemistry and Materials section of the Consortium for Advanced Radiation Sources (ChemMatCARS) beamline 15-ID at the Advanced Photon Source (APS, at Argonne National Laboratory) with measurement techniques described in detail elsewhere (*18*). The kinematics of specular reflectivity are illustrated in the inset to Fig. 1. The reflectivity data were measured as a function of the wave vector transfer normal to the interface, $Q_z = (4\pi/\lambda)\sin\alpha$ (the in-plane wave vector components $Q_x = Q_y = 0$, where $\lambda = 0.41360 \pm 0.00005$ Å is the x-ray wavelength and α is the angle of reflection). Figure 1 illustrates the reflectivity data for all of the concentrations studied.

The structure of the liquid-liquid interface is determined by the distribution of ions and solvent molecules and includes the effect of capillary wave fluctuations of the interface. X-ray reflectivity probes the electron density profile of this distribution, where the profile $\langle\rho(z)\rangle_{xy}$ is the electron density as a function of depth (along the z axis) that is averaged over the region of the x-ray footprint that lies in x-y plane of the interface. The Gouy-Chapman theory and a computer simulation were both used to predict ion distributions from which electron density profiles were computed. The reflectivity was calculated from the electron density profiles by using the Parratt formalism and then compared with the measurements (*20*).

The analytic solution to Eq. 1, when $E_i(z) = e_i\phi_i(z)$ and $\varepsilon(z) \equiv \varepsilon$, is the nonlinear Gouy-Chapman theory (*21*). The calculated ion distribution is the concentration along the interfacial normal, $c_i(z) = c_i^o \exp[-\Delta E_i(z)/k_BT]$ for ion i, and is illustrated for the 0.08 M TBABr sample (Fig. 2A). The intrinsic electron density profile $\rho_{intrinsic}(z) = \rho_{solvent} + \sum_i c_i(z)(N_i - v_i\rho_{solvent})$ is calculated from the distributions $[c_i(z)]$ for ion i, from the number of electrons (N_i) for ion i, the ion volume (v_i) in the solution, and the electron density of the solvent ($\rho_{solvent}$). The ions were modeled as spheres with diameters of 3.7 Å for Br^-, 8.6 Å for TBA^+, and 9.5 Å for TPB^-, where the charge is taken to be at the center of the sphere (*22*, *23*). The diameters for Br^- and TBA^+ were determined from our MD simulations of the radial distribution functions and are consistent with literature values (*22*). This electron density profile is referred to as an intrinsic profile because it does not include the effect of capillary waves.

The electron density profile $\langle\rho(z)\rangle_{xy}$ that includes the effect of capillary waves can be calculated by convoluting the intrinsic electron density profile with a Gaussian of width σ_{cap},

$$\langle\rho(z)\rangle_{xy} = \frac{1}{\sigma_{cap}\sqrt{2\pi}} \times \int_{-\infty}^{\infty} \rho_{intrinsic}(z')\exp[-(z - z')^2/2\sigma_{cap}^2]dz' \quad (2)$$

The interfacial width σ_{cap} is calculated from capillary wave theory by using the measured interfacial tension as described previously (*18*, *24*). The tension was measured by using a teflon Wilhelmy plate fully submerged in the water phase (Table 1). We assume that the local ion and solvent distributions are not distorted by the presence of capillary waves. This assumption is expected to be reasonable except for very short wavelength capillary waves (on the order of a bulk correlation length) or very concentrated solutions (*25*, *26*).

The electron density $\langle\rho(z)\rangle_{xy}$ calculated from the Gouy-Chapman model for the 0.08 M TBABr sample is shown in Fig. 3. Although the ion distributions in Fig. 2A are discontinuous, the electron density profile is continuous because of the effects of capillary waves.

The reflectivities calculated from the Gouy-Chapman model are shown as dashed lines in Fig. 1. This model matches the reflectivity data at the lowest concentration but progressively differs from the data with increasing concentration until reaching a difference of 25 standard deviations at the highest concentration. A variation of the Gouy-Chapman theory, the modified Verwey-Niessen model (*10*), which describes the liquid-liquid interface as consisting of two back-to-back, ion-free solvent layers that separate the Gouy-Chapman ion distributions, also fails to describe our data (*27*).

To include liquid structure in the calculation of the ion distributions, we take the energy $E_i(z)$ in Eq. 1 to be $E_i(z) = e_i\phi_i(z) + f_i(z)$. A model for $f_i(z)$ is provided by the potential of mean force calculated by MD simulations. The potential of mean force is determined by calculating the mean force on a single ion positioned at different distances from the interface between pure water and pure nitrobenzene (*18*). The exact $E_i(z)$ requires the consideration of ion-ion interactions, but this is not computationally feasible at present. Instead, we approximate $E_i(z)$ by a sum of the electrostatic term $e_i\phi_i(z)$ plus the potential of mean force for a single ion (*28*).

The potentials of mean force for TBA^+ and Br^- at the nitrobenzene-water interface are shown in Fig. 4. Ions can penetrate and transfer through a liquid-liquid interface as illustrated by the continuity of the potential of mean force in Fig. 4. The ion diameter and hydration and solvation effects contribute to the distance required for the potential of mean force

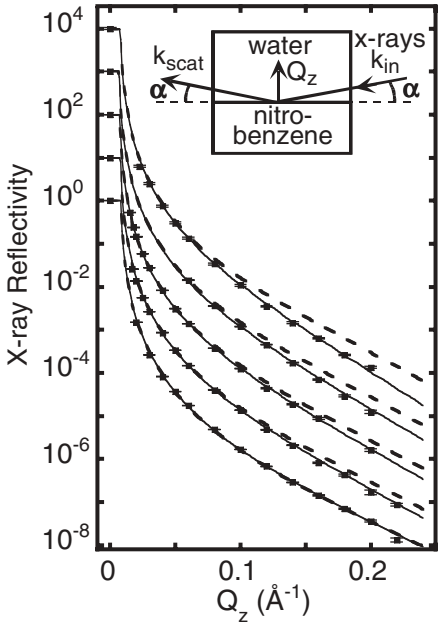

Fig. 1. X-ray reflectivity, $R(Q_z)$, as a function of wave vector transfer Q_z from the interface between a 0.01 M solution of TBATPB in nitrobenzene and a solution of TBABr in water at five concentrations (0.01, 0.04, 0.05, 0.057, and 0.08 M, bottom to top) at a room temperature of 24° ± 0.5°C. Solid lines are predictions using the potential of mean force from MD simulations. Dashed lines are predicted by the Gouy-Chapman model. No parameters have been adjusted in these two models. Data for different concentrations are offset by factors of 10 ($R = 1$ at $Q_z = 0$). Error bars are indicated by horizontal lines through the square data points and are usually much smaller than the size of the squares. The points at $Q_z = 0$ are measured from transmission through the bulk aqueous phase. **(Inset)** The kinematics of x-ray reflectivity: $\mathbf{k}_{in}$, incoming x-ray wave vector; $\mathbf{k}_{scat}$, scattered wave vector; and α, angles of incidence and reflection.

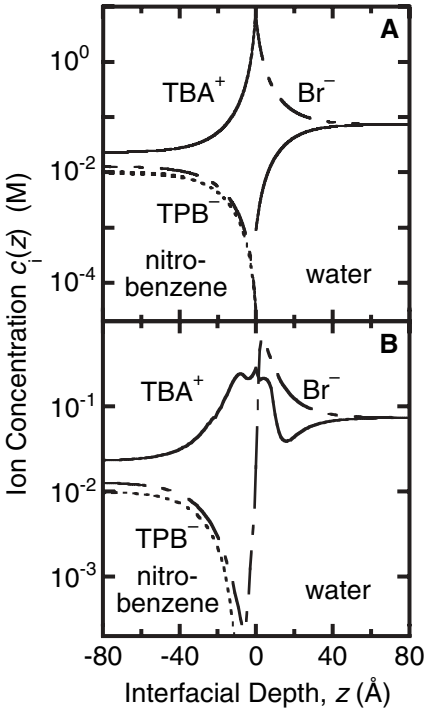

Fig. 2. Ion distributions at the interface between a 0.08 M TBABr solution in water and a 0.01 M TBATPB solution in nitrobenzene. Solid lines, TBA^+; short-long dashed line, Br^-; short dashed line, TPB^-. **(A)** Gouy-Chapman theory. **(B)** Calculation from MD simulation of the potential of mean force.

Table 1. Interfacial tension γ and capillary width of the samples. Samples are labeled by the initial concentration (in M) of TBABr in water. Tension values agree with literature measurements (*19*).

	0.01 M	0.04 M	0.05 M	0.057 M	0.08 M
γ (10^{-3} N/m) ($\pm$0.1)	19.6	15.7	14.8	14.7	13.0
σ_{cap} (Å)	5.8	6.5	6.7	6.8	7.2

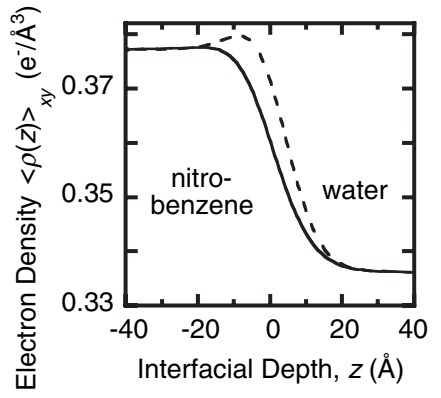

Fig. 3. Electron density, $\langle\rho(z)\rangle_{xy}$, as function of depth through the interface between a 0.08 M TBABr solution in water and a 0.01 M TBATPB solution in nitrobenzene. Dashed line, calculation from Gouy-Chapman model; solid line, calculation from MD simulation of the potential of mean force.

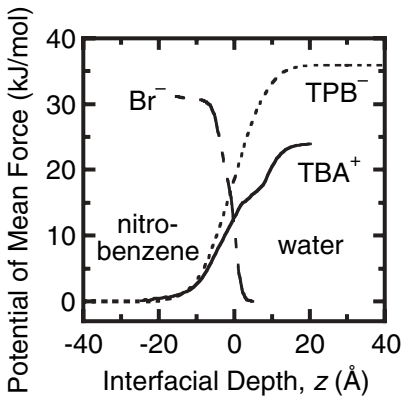

Fig. 4. Potential of mean force for TBA^+ (solid line) and Br^- (short-long dashed line) at the nitrobenzene-water interface calculated from MD simulations. The function for TPB^- (short dashed line) is provided by an analytic model (*18*). The potential of mean force for ion transfer is calculated by using the integral of the average force acting on the ion center of mass: $\Delta A = A_2 - A_1 = -\int_{z_1}^{z_2}\langle F_z(z)\rangle dz$, where F_z is the projection along the z axis of the total force acting on the ion's center of mass (*18*).

to cross from one bulk value to the other. We have not calculated the potential of mean force for TPB^- ions, so we postulated a simple functional form for TPB^- that has these qualitative features (Fig. 4) (*18*). Because the interfacial concentration of TPB^- is small, the electron density calculation is not sensitive to this function.

The electric potential $\phi(z)$ is calculated by solving Eq. 1 numerically (*29*) with the use of the functions $f_i(z)$ for TBA^+, TPB^-, and Br^- displayed in Fig. 4, setting $E_i(z) = e_i\phi_i(z) + f_i(z)$, and approximating $\varepsilon(z) \equiv \varepsilon$. Figure 2B illustrates the ion distributions calculated from $c_i(z) = c_i^o \exp[-\Delta E_i(z)/k_BT]$ for the 0.08 M TBABr sample. Lower concentrations exhibit qualitatively similar distributions but with lower ion adsorption, as expected from the variation in tension (Table 1). The distributions far from the interface are similar to those predicted by the Gouy-Chapman theory (Fig. 2A) but differ substantially in both amplitude and form near the interface. Broadening of the ion distributions at the interface is expected from the finite sizes of the ions and solvent molecules. For TBA^+, the enhanced broadening on the water side of the interface is a result of the reduced slope in the potential of mean force in that region, most likely caused by resistance of the ion to lose its hydration shell. Also, the ion distributions in Fig. 2B vary continuously across the interface because the MD simulation allows for ion penetration through the interface, in contrast to the interfacial discontinuity present in the Gouy-Chapman distributions.

The electron density profile $\langle\rho(z)\rangle_{xy}$ calculated from the ion distributions in Fig. 2B is illustrated in Fig. 3. As anticipated from the underlying ion distributions, the electron density near the interface is smaller than that predicted by the Gouy-Chapman theory. Figure 1 demonstrates that the reflectivities calculated from these electron densities match the measured reflectivities closely. We emphasize that this is not a fit and that there are no adjustable parameters. This analysis allows the data from samples of five different concentrations, which have different ion distributions, to be explained by the potentials of mean force $f_i(z)$ for each ion.

The agreement between the predictions of the MD simulation and the x-ray measurements indicates that the aspects of liquid structure included in the MD simulations, such as ion sizes and ion-solvent interactions, alter the ion distributions. The MD simulations do not include ion-ion correlations that at high concentrations are expected to lead, for example, to the formation of interfacial ion pairs. Our results suggest that these correlations do not substantially affect the ion distributions probed in this experiment, most likely because the correlations are weak at the concentrations of our samples.

This work provides a method for including liquid structure in the analysis of structural measurements of ion distributions near charged or electrified interfaces. This method allows the potentials of mean force produced by MD simulations or analytic theory to be tested by experiment. We anticipate that this method can also be applied to study ion distributions near charged solid surfaces, liquid-vapor interfaces, and the surfaces of charged biomolecules. A number of fundamental phenomena that alter the form of the potential of mean force remain to be tested at the liquid-liquid interface. These include the existence of water fingering, predicted by MD simulations to occur when strongly hydrated ions pass from the aqueous to the organic phase (*30*), and the existence of a barrier for ion transfer across the interface.

References and Notes

1. G. Gouy, *C. R. Acad. Sci.* **149**, 654 (1910).
2. D. L. Chapman, *Philos. Mag. Ser. 6* **25**, 475 (1913).
3. S. Levine, C. W. Outhwaite, L. B. Bhuiyan, *J. Electroanal. Chem.* **123**, 105 (1981).
4. J. G. Kirkwood, *J. Chem. Phys.* **2**, 767 (1934).
5. L. I. Daikhin, A. A. Kornyshev, M. Urbakh, *J. Electroanal. Chem.* **500**, 461 (2001).
6. H. H. Girault, in *Modern Aspects of Electrochemistry*, J. O. M. Bockris, Ed. (Plenum, New York, 1993), vol. 25, p. 1.
7. Z. Samec, V. Marecek, D. Homolka, *J. Electroanal. Chem.* **187**, 31 (1985).
8. C. M. Pereira, A. Martins, M. Rocha, C. J. Silva, F. Silva, *J. Chem. Soc. Faraday Trans.* **90**, 143 (1994).
9. O. Stern, *Z. Elektrochem. Angew. Phys. Chem* **30**, 508 (1924).
10. C. Gavach, P. Seta, B. d'Epenoux, *J. Electroanal. Chem.* **83**, 225 (1977).
11. M. J. Bedzyk, G. M. Bommarito, M. Caffrey, T. L. Penner, *Science* **248**, 52 (1990).
12. J. M. Bloch *et al.*, *Phys. Rev. Lett.* **61**, 2941 (1988).
13. F. Leveiller *et al.*, *Science* **252**, 1532 (1991).
14. D. Vaknin, P. Kruger, M. Losche, *Phys. Rev. Lett.* **90**, 178102 (2003).
15. P. Fenter *et al.*, *J. Colloid Interface Sci.* **225**, 154 (2000).
16. R. Das *et al.*, *Phys. Rev. Lett.* **90**, 188103 (2003).
17. K. Andresen *et al.*, *Phys. Rev. Lett.* **93**, 248103 (2004).
18. Materials and methods are available as supporting material on *Science* Online.
19. J. D. Reid, O. R. Melroy, R. P. Buck, *J. Electroanal. Chem.* **147**, 71 (1983).
20. L. G. Parratt, *Phys. Rev.* **95**, 359 (1954).
21. W. Schmickler, *Interfacial Electrochemistry* (Oxford Univ. Press, Oxford, 1996).
22. H. Ohtaki, T. Radnai, *Chem. Rev.* **93**, 1157 (1993).
23. B. S. Krumgalz, *J. Chem. Soc. Faraday Trans.* **78**, 437 (1982).
24. D. M. Mitrinovic, A. M. Tikhonov, M. Li, Z. Huang, M. L. Schlossman, *Phys. Rev. Lett.* **85**, 582 (2000).
25. K. R. Mecke, S. Dietrich, *Phys. Rev. E* **59**, 6766 (1999).
26. L. I. Daikhin, A. A. Kornyshev, M. Urbakh, *J. Electroanal. Chem.* **483**, 68 (2000).
27. G. Luo *et al.*, data not shown.
28. Both $\phi(z)$ and $f(z)$ include the potential drop due to the neat liquid-liquid interface. We assume that the potential drop across the neat interface is much smaller than that produced by the ions.
29. D. M. Burley, V. C. L. Hutson, C. W. Outhwaite, *Mol. Phys.* **23**, 867 (1972).
30. I. Benjamin, *Science* **261**, 1558 (1993).

31. M.L.S. and P.V. acknowledge support from NSF-CHE0315691, and I.B. acknowledges support from NSF-CHE0345361. M.L.S. thanks J. Gebhardt, T. Graber, and H. Brewer for help with the ChemMatCARS ID beamline and B. Hou for assisting with the x-ray measurements. ChemMatCARS is supported by NSF-CHE, NSF-DMR, and the U.S. Department of Energy (DOE). The APS is supported by the DOE Office of Basic Energy Sciences.

Supporting Online Material

www.sciencemag.org/cgi/content/full/311/5758/216/DC1
Materials and Methods
Fig. S1
Table S1

20 September 2005; accepted 30 November 2005
10.1126/science.1120392

Ion Distributions near a Liquid-Liquid Interface

Guangming Luo, Sarka Malkova, Jaesung Yoon, David G. Schultz, Binhua Lin, Mati Meron, Ilan Benjamin, Petr Vanýsek and Mark L. Schlossman (January 13, 2006)

Science **311** (5758), 216-218. [doi: 10.1126/science.1120392]

Editor's Summary